

Log-Likelihood Score Level Fusion for Improved Cross-Sensor Smartphone Periocular Recognition

Fernando Alonso-Fernandez*, Kiran B. Raja †, Christoph Busch †, Josef Bigun *

*Halmstad University. Box 823. SE 301-18 Halmstad, Sweden

Email: {feralo, josef.bigun}@hh.se

† Norwegian University of Science and Technology, Gjøvik, Norway

Email: {kiran.raja, christoph.busch}@ntnu.no

Abstract—The proliferation of cameras and personal devices results in a wide variability of imaging conditions, producing large intra-class variations and a significant performance drop when images from heterogeneous environments are compared. However, many applications require to deal with data from different sources regularly, thus needing to overcome these interoperability problems. Here, we employ fusion of several comparators to improve periocular performance when images from different smartphones are compared. We use a probabilistic fusion framework based on linear logistic regression, in which fused scores tend to be log-likelihood ratios, obtaining a reduction in cross-sensor EER of up to 40% due to the fusion. Our framework also provides an elegant and simple solution to handle signals from different devices, since same-sensor and cross-sensor score distributions are aligned and mapped to a common probabilistic domain. This allows the use of Bayes thresholds for optimal decision making, eliminating the need of sensor-specific thresholds, which is essential in operational conditions because the threshold setting critically determines the accuracy of the authentication process in many applications.

I. INTRODUCTION

The periocular region, the area surrounding the eye, has shown a surprisingly high discrimination ability, while requiring the least constrained acquisition among ocular or facial modalities [1]. It has thus become a very popular modality due to the proliferation of unconstrained or uncooperative scenarios, e.g. surveillance or smartphones [2]. However, this massive availability of devices results in heterogeneous quality between probe and gallery images, which is known to reduce performance significantly when different capture devices are used [3]. Even if the sensors work in the same spectrum, they may have different spatial sampling rate, illumination sources, field of view, etc. thus resulting in a challenge of interoperability despite operating in the same spectrum [4].

This paper evaluates the fusion of different recognition systems to improve cross-sensor recognition of images from different smartphones. We use five periocular comparators based on popular features from the literature, and the Visible Spectrum Smartphone Iris (VSSIRIS) database [5], containing images from two smartphones. The individual comparators provide accurate recognition when comparing images from the same device (with EER~0%), but a 4- to 10-fold EER increase is observed if images are not from the same device. There is also correlation between their performance and the size of extracted templates. While the most accurate comparator

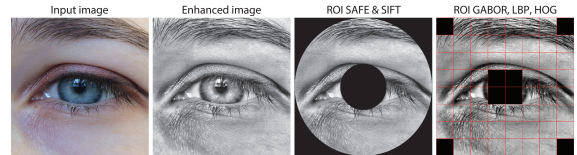


Fig. 1. Example image from VSSIRIS database. First/second columns: input/preprocessed image with CLAHE. Third: ROI of SAFE and SIFT comparators. Fourth: ROI of GABOR, LBP and HOG comparators (for consistency with SAFE/SIFT, center and corner blocks are discarded).

provides ~0% EER, it has a template size and comparison time that might be prohibitive for real-time recognition in devices with limited processing capabilities. Fusion improves cross-sensor EER in more than 40%, demonstrating the validity of the proposed approach. We employ a trained fusion based on linear logistic regression [6], in which scores are mapped to log-likelihood-ratios. As a result, scores are in the same probabilistic, sensor-independent domain, regardless whether they come from comparison trials from same-sensor or different-sensor images, greatly simplifying the fusion process.

The rest of the paper is as follows. The periocular comparators employed are described in Section II. Section III describes the database and experimental protocol. Results of individual comparators and fusion experiments are presented in Sections IV and V, respectively. Conclusions are given in Section VI.

II. PERIOCLAR RECOGNITION SYSTEMS

This section describes the five machine experts evaluated.

Symmetry Patterns based on the Symmetry Assessment by Feature Expansion (**SAFE**) descriptor [7], which encodes the presence of various symmetric curve families in concentric annular rings around image key-points. We use the sclera center as unique key-point. The system employs 6 different scales for feature extraction, with 3 disjoint rings and 9 symmetry families per scale. The first annular ring starts at the sclera circle, and the last ends at the image boundary. The ROI is shown in Figure 1 (third column). The sclera is used as anchor point, both to compute the eye center and to estimate the ROI, due to its invariance to iris dilation.

Gabor Features (GABOR). The image is decomposed into non-overlapped blocks (Figure 1, fourth column), and the

local power spectrum is then sampled at the center of each block by a set of Gabor filters organized in 5 frequency and 6 orientation channels [8]. This sparseness of the sampling grid allows direct filtering in the image domain without needing the Fourier transform, with significant computational savings.

SIFT key-points (SIFT) [9] with the adaptations described in [10] for iris images, particularly a post-processing step to remove spurious keypoints using geometric constraints.

Local Binary Patterns (LBP) and Histogram of Oriented Gradients (HOG). Together with SIFT key-points, LBP [11] and HOG [12] are the most widely used features in periocular research [2]. The image is decomposed into non-overlapped regions (Figure 1). Then, HOG and LBP features are extracted from each block, quantized into 8 different values (8 bins histogram) per block, with histograms further normalized to account for local illumination and contrast variations.

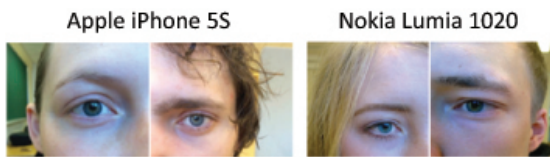


Fig. 2. Sample images from VSSIRIS database (taken from [5]).

III. DATABASE AND EXPERIMENTAL PROTOCOL

We use the Visible Spectrum Smartphone Iris (VSSIRIS) database [5], having 28 semi-cooperative subjects (56 eyes) captured indoors with two smartphones (iPhone 5S and Nokia Lumia 1020, with images of 3264×2448 and 3072×1728 pixels, respectively), without flash. Each eye has 5 samples per smartphone, so $5 \times 56 = 280$ images per device are available. Figure 2 shows some examples. All images are annotated manually, so radius and center of the iris circles are available. Images are resized by bicubic interpolation to have the same sclera radius ($R=145$, average of the database), then they are aligned by extracting a region of $6R \times 6R$ (871×871) around the sclera center. This size is set empirically to ensure that all images have sufficient margin to the four sides. We use the sclera for normalization since it is not affected by dilation. Images are further equalized with CLAHE [13] to compensate local illumination variability (Figure 1).

We carry out verification experiments, comparing images both from the same device (*same-sensor*) and different devices (*cross-sensor*). Each eye is considered a different instance. Genuine comparison trials are done by comparing each image of an instance to the remaining images of the same eye, avoiding symmetric comparisons. This results in $10 \times 56 = 560$ (same-sensor) and $5 \times 5 \times 56 = 1400$ (cross-sensor) scores per smartphone. Impostor trials are done by comparing the 1st image of an instance to the 2nd image of the remaining eyes, resulting in $56 \times 55 = 3080$ scores both in same- and cross-sensor tests. Experiments have been done in a Dell E7240 laptop (i7-4600 processor, 16 Gb DDR3 RAM, built-in Intel

HD Graphics 4400) with MS Windows 8.1 Pro. The algorithms are implemented in Matlab r2009b x64, with the exception of SIFT that is in C++¹ and invoked from Matlab via MEX files. Size of stored template files and the extraction and matching computation times are given in Table I.

system	Template Size	Extraction Time	Comparison Time
SAFE	4.4 Kb	11.86 sec	<0.1 msec
GABOR	25.5 Kb	0.53 sec	0.3 msec
SIFT	2138 Kb	1.5 sec	1.1 sec
SIFT 200p	115.7 Kb	-	6.1 msec
SIFT 100p	58.1 Kb	-	2 msec
LBP	3.2 Kb	0.17 sec	<0.1 msec
HOG	3.6 Kb	0.13 sec	<0.1 msec

TABLE I
SIZE OF THE TEMPLATE FILE AND COMPUTATION TIMES.

IV. RESULTS: INDIVIDUAL SYSTEMS

Performance is reported in Figures 3 and 4. EER values are also given in Table II. We report: *i) same-sensor* comparison; *ii) cross-sensor* comparison; and *iii) overall* (pooling scores of *i* and *ii*). We use the SIFT detector as in [10] for iris images, but here it gives ~ 3000 key-points per image due to a much bigger ROI. This allows an EER of $\sim 0\%$ in same-sensor comparisons, but the template has several MBs and comparison time is >1 sec on a laptop in C++ (Table I), which may not be feasible if transferred to devices with limited capabilities. Comparison time is one of the drawbacks of key-point based systems, since it is usually needed to compare each key-point of one image against all key-points of the other. The other comparators employed have templates of fixed size, thus comparison is very efficient. For this reason, we also report results limiting the key-points per image to 100 and 200 (by changing the threshold to exclude low contrast points), an approach observed in other studies when image resolution increases [14]. The SIFT comparator with 100 key-points still has a template and a comparison time one order of magnitude bigger than some other systems, but similar performance or even worse. This indicates that the most n salient key-points of one image do not necessarily pair fully with the most n salient key-points of other image from the same eye instance, so this limiting approach may not be an efficient solution either.

From Figure 3 and Table II, we observe that even if performance of same-sensor experiments can be very good, cross-sensor comparison results in a significant worsening. There is also correlation between a bigger template (Table I) and lower EER (Table II). It is worth noting too the comparable performance of SAFE w.r.t. GABOR, with template one fourth in size. Also, SAFE, LBP and HOG templates are comparable, but performance of the two latter comparators are worse. This reflects the discriminative capability of SAFE filters, although at the expense of a higher extraction time, since convolution filters are of similar size than the input image

¹<http://vision.ucla.edu/~vedaldi/code/sift/assets/sift/index.html>

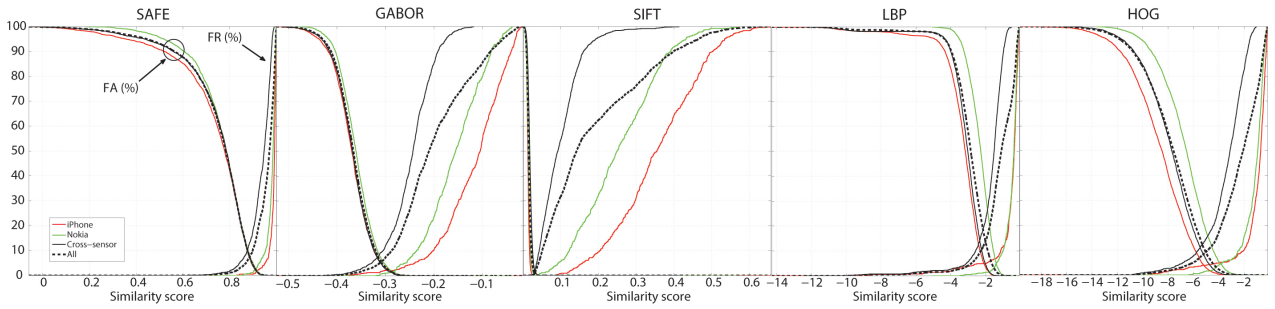


Fig. 3. Verification results of the individual systems (DET curves).

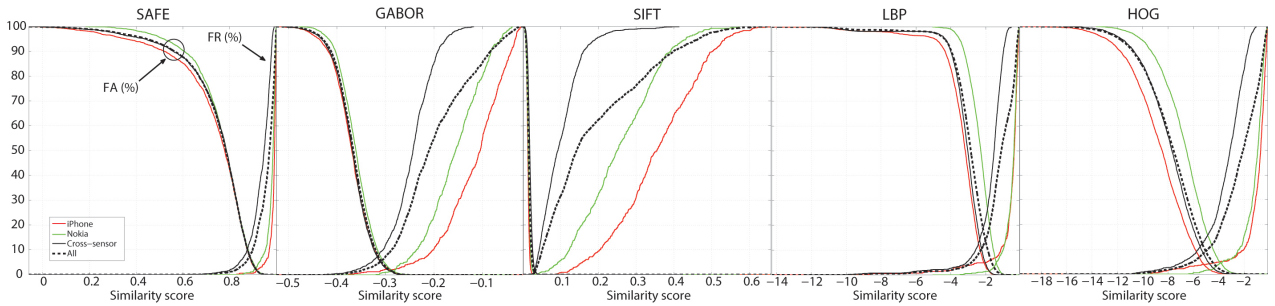


Fig. 4. Verification results of the individual systems (FA, FR curves).

(871×871). However, filter separability could be explored for faster processing [8]. An interesting observation from Figure 4 is that in the cross-sensor scenario, genuine score distributions (FR curve) shift significantly towards the impostor distribution (FA), whereas impostor distributions remain in the same range (at least with SAFE, GABOR and SIFT). This means that ‘similarity’ between images of the same instance is reduced when they come from a different sensor, at least measured by the features employed. It is also interesting that same-sensor performance is not similar for each sensor, even if they involve the same eyes, and images have the same size. Genuine score distributions are also observed to be in a different range for each sensor (red and green FR curves of Figure 4). We apply local adaptive contrast equalization, but results suggest however that other device-dependant processing might be of help to compensate variations in performance [15].

system	iPhone	Nokia	cross-sensor	all
SAFE	1.6%	2.6%	10.2%	7.5%
GABOR	2.1%	1.5%	7.3%	5.8%
SIFT	0%	0.1%	1.6%	0.8%
SIFT 200p	0%	0.8%	6.6%	5%
SIFT 100p	0.1%	2.1%	11.9%	8%
LBP	4.8%	4.9%	14.1%	13.8%
HOG	3.9%	4.5%	11%	9.2%

TABLE II
VERIFICATION RESULTS OF THE INDIVIDUAL SYSTEMS (EER).

V. RESULTS: FUSION OF PERIOULAR SYSTEMS

We carry out fusion experiments using all the available comparators. Given N comparators which output scores

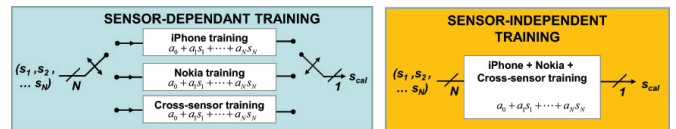


Fig. 5. Architecture of the two fusion strategies implemented.

$S=(s_1, s_2, \dots, s_N)$ for an input trial, a linear fusion is: $s_{cal} = a_0 + a_1 \cdot s_1 + \dots + a_N \cdot s_N$. Weights a_0, a_1, \dots, a_N are trained via logistic regression following a probabilistic Bayesian framework [6], in a way that $s_{cal} \simeq \log(p(S|\omega_i)/p(S|\omega_j))$. This is the logarithm of the ratio between the likelihood that input signals are originated by the same eye instance (target hypothesis ω_i) or not (non-target hypothesis ω_j). An advantage of this approach is that s_{cal} has a probabilistic value by itself, representing a *degree of support* to any of the ω_i and ω_j hypotheses: if it is higher than 0, then the support to ω_i is higher, and vice-versa. This trained approach has also shown better performance than simple fusion rules (like mean or sum) in previous works, and presents advantages too when signals originate from heterogeneous sources [6], as shown next.

We evaluate two fusion strategies (Figure 5): *i*) *sensor-dependant*, with a fusion function trained separately for *same-sensor* (one per device) and *cross-sensor* scores; and *ii*) *sensor-independent*, with a unique fusion function trained with same- and cross-sensor scores together. Case *i*) implies that the device is known, which is reasonable in operational scenarios, while case *ii*) does not exploit any knowledge regarding the device used to capture signals. We have tested all possible fusion combinations, with the best results reported in Table III.

The best combinations are chosen based on the lowest cross-sensor EER. As it can be observed, fusion improves cross-sensor performance significantly, with more than 40% EER reduction if the local SIFT comparator is involved; if not (bottom part of Table III), cross-sensor performance still improves 14-18%. Regarding the two fusion strategies evaluated, there is no substantial difference in cross-sensor EER, but performance of same-sensor tests is equal or better by using sensor-dependant training. This is because training is done optimally for each sensor, tailored to differences in the range of similarity scores observed (Figure 4). A further benefit is that same- and cross-sensor score distributions are aligned after the fusion (Figure 6), providing an elegant and simple solution for handling signals from different devices, since there is no need of sensor-specific thresholds. As a result, global performance as computed by pooling all scores together (columns ‘all’ in Table III) is significantly better as well.

It can also be seen (Table III) that the best performance is not necessarily obtained by using all available systems. Indeed, the highest improvement occurs after the fusion of two or three systems. Inclusion of more systems produces smaller improvements (or no improvement at all). The best performance is given by fusion of only two systems (SAFE, SIFT), with a cross-sensor EER reduction from 1.6% to 0.9% (even if the cross-sensor performance of SAFE is 10.2%). Optimal combinations always involve the SIFT comparator, which also has the best individual performance (or among the bests when the number of key-points is limited). The good performance of SIFT is not jeopardized during the fusion by other comparators with a performance an order of magnitude worse, but it is complemented to obtain even better same- and cross-sensor EERs. This is because in the trained fusion approach employed, the support of each modality is implicitly weighted by its accuracy. In other simple fusion methods (such as mean or sum of scores), all comparator are given the same weight independently of its accuracy. This is a common problem of these methods, that makes the worst modalities to yield misleading results more frequently [16].

A careful look at the best combinations of Table III shows that SAFE or GABOR comparator are always chosen first for the fusion. Together with SIFT, these are very powerful descriptors that capture different image features, thus being very complementary too. If we eliminate SIFT from the equation (bottom of Table III), a cross-sensor performance of $\sim 6\%$ can be still obtained with the available systems, while keeping same-sensor performance below 1.5%.

VI. CONCLUSIONS

As biometric technology is increasingly deployed, it will be common to compare signals from different devices in mismatched conditions. This issue, known as device interoperability, is known to reduce performance significantly [17]. We propose the log-likelihood score fusion of several comparators to improve cross-sensor periocular performance using images from different smartphones. We evaluate five periocular descriptors of wide use in the literature. The database employed

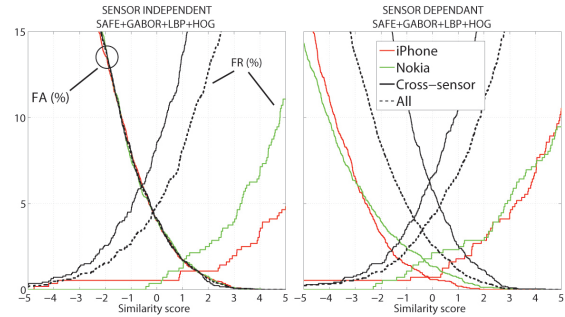


Fig. 6. Verification results of a fusion example (FA, FR curves). Left: fusion training is done by pooling same- and cross-sensor scores; as a result, misalignment between these cases exist. Right: separate training allows the score distributions to be centered around a log-likelihood ratio of 0.

has 560 periocular images from two smartphones. The fusion scheme is based on linear logistic regression [6], in a way that output scores are mapped to log-likelihood-ratios, thus being in an sensor-independent domain.

Even if the performance when comparing images from the same sensor can be very good (down to $\sim 0\%$ with one comparator), an EER increase of 4 to 10 times is observed when comparing images from different smartphones. Score distributions reveal that the ‘similarity’ between images of the same eyes instance is reduced when they come from a different sensor, measured by a shift in the genuine scores distribution towards a range of smaller similarity values. An increased intra-class variability is expected in cross-comparison conditions, due to variability introduced by different imaging devices [6]. For fusion experiments, we consider two strategies (Figure 5), one that estimates a different training model for each sensor (sensor-dependent), and another that trains a single fusion model by pooling both same-sensor and cross-sensor scores together. A reduction in cross-sensor performance of more than 40% can be achieved with the fusion, with the sensor-dependent strategy providing additional advantages. For example, since the fusion function is optimized for each sensor, better performance is obtained when comparing images from the same device. A further advantage is that same- and cross-sensor score distributions are aligned after the fusion, avoiding the use of sensor-specific decision thresholds and providing significantly better global performance as well.

Future work includes the use of device-dependant image preprocessing to compensate variations in image properties [15]. The proposed framework can be applied to comparison of images from different spectra too [3]. In the context of smartphone recognition, where high resolution images are usual, fusion with the iris modality is another possibility [18]. However, it requires segmentation, which might be an issue if the image quality is not sufficiently high, which also motivates pursuing the periocular modality, as in the current study. We will also validate our methodology using databases not only limited to two devices, and also including more extreme variations in camera specifications and imaging conditions.

USING ALL THE SYSTEMS AVAILABLE

SENSOR-INDEPENDENT TRAINING							SENSOR-DEPENDANT TRAINING												
# systems	safe	gabor	sift	lbp	hog	iphone	nokia	cross-sensor	all	# systems	safe	gabor	sift	lbp	hog	iphone	nokia	cross-sensor	all
1						0	0.1	1.6	0.8	1						0	0.1	1.6	0.8
2	x	x				0 (0%)	0 (-100%)	0.9 (-43.8%)	0.4 (-50%)	2	x	x				0 (0%)	0 (-100%)	0.9 (-43.8%)	0.4 (-50%)
3	x		x			0 (0%)	0 (-100%)	0.9 (-43.8%)	0.4 (-50%)	3	x		x			0 (0%)	0 (-100%)	0.9 (-43.8%)	0.4 (-50%)
4	x	x	x			0 (0%)	0 (-100%)	0.9 (-43.8%)	0.4 (-50%)	4	x	x	x			0 (0%)	0 (-100%)	0.9 (-43.8%)	0.4 (-50%)
5	x	x	x	x		0 (0%)	0 (-100%)	0.9 (-43.8%)	0.4 (-50%)	5	x	x	x	x		0 (0%)	0 (-100%)	0.9 (-43.8%)	0.4 (-50%)
					best	0	0	0.9	0.4						best	0	0	0.9	0.4

USING LOCAL SIFT COMPARATOR RESTRICTED TO 200 KEY-POINTS PER IMAGE

SENSOR-INDEPENDENT TRAINING							SENSOR-DEPENDANT TRAINING												
# systems	safe	gabor	sift 200p	lbp	hog	iphone	nokia	cross-sensor	all	# systems	safe	gabor	sift	lbp	hog	iphone	nokia	cross-sensor	all
1						0	0.8	6.6	5	1						0	0.8	6.6	5
2	x	x				0 (0%)	0.5 (-37.5%)	3.1 (-53%)	2.7 (-46%)	2	x	x				0 (0%)	0.5 (-37.5%)	3.1 (-53%)	1.4 (-72%)
3	x	x	x			0 (0%)	0.4 (-50%)	2.9 (-56.1%)	2.5 (-50%)	3	x	x	x			0 (0%)	0.5 (-37.5%)	2.8 (-57.6%)	1.4 (-72%)
4	x	x	x	x		0 (0%)	0.4 (-50%)	3 (-54.5%)	2.3 (-54%)	4	x	x	x	x		0 (0%)	0.3 (-62.5%)	2.8 (-57.6%)	2.1 (-58%)
5	x	x	x	x	x	0 (0%)	0.4 (-50%)	3 (-54.5%)	2.2 (-56%)	5	x	x	x	x	x	0 (0%)	0.3 (-62.5%)	2.9 (-56.1%)	1.3 (-74%)
					best	0	0.4	2.9	2.2						best	0	0.3	2.8	1.3

USING LOCAL SIFT COMPARATOR RESTRICTED TO 100 KEY-POINTS PER IMAGE

SENSOR-INDEPENDENT TRAINING							SENSOR-DEPENDANT TRAINING												
# systems	safe	gabor	sift 100p	lbp	hog	iphone	nokia	cross-sensor	all	# systems	safe	gabor	sift	lbp	hog	iphone	nokia	cross-sensor	all
1						0.1	1.5	7.3	5.8	1						0.1	1.5	7.3	5.8
2	x	x				0.3 (+200%)	1.2 (-20%)	4.9 (-32.9%)	3.8 (-34.5%)	2	x	x				0 (-100%)	1.2 (-20%)	4.9 (-32.9%)	2.5 (-56.9%)
3	x	x	x			0.3 (+200%)	0.9 (-40%)	4.6 (-37%)	3.5 (-39.7%)	3	x	x	x			0 (-100%)	0.9 (-40%)	4.7 (-35.6%)	2.2 (-62.1%)
4	x	x	x	x		0.3 (+200%)	0.9 (-40%)	4.2 (-42.5%)	3.3 (-43.1%)	4	x	x	x	x		0 (-100%)	0.9 (-40%)	4.2 (-42.5%)	2.1 (-63.8%)
5	x	x	x	x	x	0.3 (+200%)	0.9 (-40%)	4.4 (-39.7%)	3.4 (-41.4%)	5	x	x	x	x	x	0 (-100%)	0.9 (-40%)	4.3 (-41.1%)	2.1 (-63.8%)
					best	0.2	0.9	4.2	3.3						best	0	0.9	4.2	2.1

WITHOUT LOCAL SIFT COMPARATOR

SENSOR-INDEPENDENT TRAINING							SENSOR-DEPENDANT TRAINING											
# systems	safe	gabor	lbp	hog	iphone	nokia	cross-sensor	all	# systems	safe	gabor	lbp	hog	iphone	nokia	cross-sensor	all	
1					2.1	1.5	7.3	5.8	1					2.1	1.5	7.3	5.8	
2	x	x			1.6 (0%)	1.8 (+20%)	6.9 (-5.5%)	5.2 (-10.3%)	2	x	x			1.2 (-25%)	1.8 (+20%)	6.9 (-5.5%)	4 (-31%)	
3	x	x	x		1.1 (-31.3%)	1.8 (+20%)	6.2 (-15.1%)	4.8 (-17.2%)	3	x	x	x		0.9 (-43.8%)	1.8 (+20%)	6.3 (-13.7%)	3.5 (-39.7%)	
4	x	x	x	x	1.1 (-31.3%)	1.6 (+6.7%)	6 (-17.8%)	4.5 (-22.4%)	4	x	x	x	x	0.7 (-56.3%)	1.8 (+20%)	6.3 (-13.7%)	3.5 (-39.7%)	
					best	1.1	1.5	6	4.5					best	0.7	1.5	6.3	3.5

TABLE III

VERIFICATION RESULTS IN TERMS OF EER (IN %) FOR AN INCREASING NUMBER OF FUSED SYSTEMS. THE BEST EER ACHIEVED FOR EACH CASE IS GIVEN, TOGETHER WITH THE SYSTEMS INVOLVED IN THE FUSION (BEST COMBINATIONS ARE CHOSEN BASED ON THE LOWEST EER OF CROSS-SENSOR EXPERIMENTS). THE RELATIVE EER VARIATION WITH RESPECT TO THE BEST INDIVIDUAL SYSTEM IS GIVEN IN BRACKETS. IT IS ALSO REPORTED THE FUSION OF 3 SYSTEMS BASED ON SIFT, LGP AND HOG, USED AS REFERENCE IN MANY PERIOULAR STUDIES [2].

ACKNOWLEDGMENT

This work was done while F. A.-F. was a visiting researcher at the Norwegian University of Science and Technology in Gjøvik (Norway), funded by EU COST Action IC1106. F. A.-F. and J. B. also than the Swedish Research Council, and the CAISR and SIDUS-AIR programs of the Swedish Knowledge Foundation.

REFERENCES

- [1] I. Nigam, M. Vatsa, R. Singh, "Ocular biometrics: A survey of modalities and fusion approaches," *Information Fusion*, vol. 26, 2015.
- [2] F. Alonso-Fernandez and J. Bigun, "A survey on periocular biometrics research," *Pattern Recognition Letters*, vol. 82, 2016.
- [3] R. R. Jillela, A. Ross, "Matching face against iris images using periocular information," *Proc Intl Conf Image Processing, ICIP*, 2014.
- [4] A. Jain, K. Nandakumar, A. Ross, "50 years of biometric research: Accomplishments, challenges, and opportunities," *Patt Rec Lett*, 2016.
- [5] K. B. Raja, R. Raghavendra, V. K. Vemuri, C. Busch, "Smartphone based visible iris recognition using deep sparse filtering," *Patt Recogn Lett*, vol. 57, pp. 33-42, 2015.
- [6] F. Alonso-Fernandez, J. Fierrez, D. Ramos, J. Gonzalez-Rodriguez, "Quality-based conditional processing in multi-biometrics: Application to sensor interoperability," *IEEE TSMC-A*, vol. 40, no. 6, 2010.
- [7] F. Alonso-Fernandez, A. Mikaelyan, J. Bigun, "Compact Multi-Scale Periocular Recognition Using SAFE Features," *Proc ICPR*, 2016.
- [8] F. Alonso-Fernandez, J. Bigun, "Near-infrared and visible-light periocular recognition with gabor features using frequency-adaptive automatic eye detection," *IET Biometrics*, vol. 4, no. 2, pp. 74-89, 2015.
- [9] D. Lowe, "Distinctive image features from scale-invariant key points," *Intl Journal of Computer Vision*, vol. 60, no. 2, pp. 91-110, 2004.
- [10] F. Alonso-Fernandez, P. Tome-Gonzalez, V. Ruiz-Albacete, J. Ortega-Garcia, "Iris recognition based on sift features," *Proc BIDS*, 2009.
- [11] T. Ojala, M. Pietikainen, T. Maenpaa, "Multiresolution gray-scale and rotation invariant texture classification with local binary patterns," *IEEE TPAMI*, vol. 24, no. 7, pp. 971-987, 2002.
- [12] N. Dalal, B. Triggs, "Histograms of oriented gradients for human detection," *Proc CVPR*, 2005.
- [13] K. Zuiderveld, "Graphics gems iv," pp. 474-485, 1994. [Online]. Available: <http://dl.acm.org/citation.cfm?id=180895.180940>
- [14] C. Padole, H. Proenca, "Periocular recognition: Analysis of performance degradation factors," *Proc ICB*, 2012.
- [15] G. Santos, E. Grancho, M. V. Bernardo, P. T. Fiadeiro, "Fusing iris and periocular information for cross-sensor recognition," *Patt Rec Lett*, 2014.
- [16] A. Jain, K. Nandakumar, A. Ross, "Score Normalization in Multimodal Biometric Systems," *Patt Recogn*, vol. 38, no. 12, 2005.
- [17] A. K. Jain, A. Kumar, *Second Generation Biometrics*. Springer, 2010, ch. Biometrics of Next Generation: An Overview.
- [18] F. Alonso-Fernandez, A. Mikaelyan, J. Bigun, "Comparison and fusion of multiple iris and periocular matchers using near-infrared and visible images," *Proc IWBF*, 2015.